P- glycoprotein (P-gp) Mediated Drug Interaction between Digoxin & Orange Juice - An Exploratory Study by *in-silico* Approach

Deepalakshmi M[1*], Arun K P[1], Srikanth Jupudi[2], Akila A[1], Kailash Kumar S[1], Sanjay V[1], Yogesh V[1]

[1]Department of Pharmacy Practice, JSS College of Pharmacy, JSS Academy of Higher Education & Research, The Nilgiris, Tamil Nadu, India.
[2]Department of Pharmaceutical Chemistry, JSS College of Pharmacy, JSS Academy of Higher Education & Research, The Nilgiris, Tamil Nadu, India.
Email: [1]deepapharmacy@jssuni.edu.in, [1]kparun@jssuni.edu.in,[1]sjphd@jssuni.edu.in, [1]akilaandazhagan2001@gmail.com, [1]kailashkumarsridevi@gmail.com, [1]sanjayvasanth5564@gmail.com, [1]yogeshvenkatesan77@gmail.com
Corresponding Author (*): Deepalakshmi M

Abstract

Background - The aim of this study explores the potential interaction between digoxin and orange juice through a P-glycoprotein (P-gp)-mediated pathway using in-silico methods. The primary goals are to identify components in orange juice that inhibit P-gp, potentially reducing digoxin's serum toxicity, and to compare the effectiveness of these components with standard P-gp inhibitors such as ketoconazole.

Methods - Molecular docking studies were performed to assess the binding affinity of various orange juice constituents to P-gp. The binding energies of these components, including hesperidin, were evaluated, and the highest affinity was determined. Vicenin-26”-O-glucoside from orange juice demonstrated the highest binding affinity to P-gp, suggesting its strong inhibitory potential.

Results - The results indicate that orange juice may serve as a moderate but effective P-gp inhibitor, comparable to ketoconazole.

Conclusion - Orange juice, particularly through its constituent vicenin-26”-O-glucoside, shows potential as a P-gp inhibitor and could reduce digoxin toxicity, offering a natural alternative to existing pharmaceutical inhibitors like ketoconazole.

Keywords: P-glycoprotein, In-silico, Molecular docking, Drug interaction.

Introduction

In 1973 Keld Dano showed that the decreased levels of drug accumulation in tumor cells was energy dependent [(1)]. P-gp was primarily named as permeability (P)- glycoprotein because it caused drug resistance by making the cellular membrane less permeable which was identified by Juliano and Ling in 1976 [(2)]. The molecular structure of human P-glycoprotein in the ATP-bound is an outward facing conformation which comes under the classification of transport protein. For many decades, the structures of inward facing conformation of P-gp are available but now the structure of the human P-gp in outward -facing conformation has been determined

by electron cryomicroscopy at 3.4 A of resolution [3]. P-gp effluxes Xenobiotics and other drugs from cells through ATP-powered conformational changes [4].

P-glycoprotein is an ATP-binding cassette exporter responsible for drug resistance to chemotherapy. The ABC transporters can be classified into seven subfamilies (ABCA-ABCG) based on their sequence homology and domain organization. These transporters consist of minimally four domains: two nucleotide -binding domains (NBD's) with sequence motifs and two transmembrane domains. The P-gp is around 170 KDa which is coded by ABCB1 (MDR1) gene, which is overexpressed in the cancer cells of tumors treated by anti-cancer drugs [5].

Non-polar compounds are usually expelled from the cytosolic environment of the membrane bilayer to the extracellular environment. Other efflux transporters which cause MDR are encoded by ABCC1-6 genes and ABCG2 gene. Many membrane "barriers" like Blood Brain Barrier, gastrointestinal tract, kidney, liver, ovary, and the placenta are the membranes where P-gp is expressed. P-gp protects sensitive tissues and the fetus from endogenous and exogenous toxicity which can be identified as its main physiological function [6].

The mechanism of P-gp in the cancer cells is that the efflux of the drugs from the tumor cells through the ATP binding cassette (ABC) transporters, which act as integral membrane pumps [7]. There are two active ATPase sites, but only one ATP is hydrolyzed at a time. The transport cycle of the substrates (drugs) which are bound to the transmembrane binding pocket in an inward facing conformation of P-gp is converted into an outward facing conformation that can release the substrates to extracellular environment which happened due to the hydrolysis of ATP, and enabled by the dimerization of NBD's that led to the outward facing conformation in the first place, it comes back to the initial inward facing state and closes the cycle [8]. There are two nucleotide binding domains which form a closed dimer occluding two ATP molecules.

P-gp is often expressed on the apical membranes of kidney epithelial cells. Its role in restricting the xenobiotic absorption by extruding its drugs from the cells into the proximal tubule [9].

Cancer cells develop resistance to chemically diverse compounds, and this is known as multi drug resistance. Multidrug resistance causes therapeutic failure not only in cancer but also in other diseases [10]. Almost three generations of MDR inhibitors have been introduced in clinical trials over the last few decades to overcome MDR. The effects of orange juice on drug transport by MDR1 protein, also known as efflux transporters, are expressed in the kidney epithelial cells [11]. There are different types of P-gp like the P-gp present in mouse, human, Cyanidioschyzon Merolae P-gp and C.Elegans P-gp. Homology models of human P-gp in which some of them had different properties than the mouse homology arising from sequence variation [12]. There is no crystal structure of the human P-gp to date hence most of the P-gp modulators have used the mouse variant of that protein. It acts as a good surrogate for the human variant due to high homology of 87% [13]. 6C0V is the human P-gp that contains small molecules like ATP and magnesium ion. The macromolecule content like total structure weight of human P-gp is 143.72 KDa. P-gp consists of two ATPase sites, each comprising the walker A/B motif of the one NBD and the LSGGQ motif of the other NBD [14].

Each ATPase site has glutamate residue that acts as the catalytic base for ATP hydrolysis and mutating the glutamate severely reduces the ATPase activity so the mutant P-gp generated was having glutamines which replaced both the catalytic glutamates [15]. The p-gp has a PH level to be maintained around PH value of 7.4. P-gp has at least two positively cooperative sites for drug binding with the H site preferring Hoechst 33342 to rhodamine 123 and the R site preferring rhodamine 123 to Hoechst 33342. Binding to one site stimulates the binding to the

other and respective transport activity. Others like M site- Modulator binding site have been reported to be seen and assigned in P-gp [16].

The P-gp substrates are:

Pharmacological classification - Drugs

Antacids - Cimetidine, Ranitidine

Antiemetic - Ondansetron

Anti-tumor - Paclitaxel, Vincristine, Doxorubicin, Vinblastine, Imatinib.

Beta-Adrenoreceptor antagonist - Reserpine

Immunosuppressants - Cyclosporin, Sirolimus

Cardiac drugs/Anti-arrhythmic – Digoxin [17]

The molecular weight of Digoxin is 780.9, log P value is around 1.26. it is sparingly soluble to insoluble in water and freely soluble to slightly soluble in alcohol or diluted alcohol. P-gp located on cells in the intestine, may interfere with digoxin pharmacokinetics as it is a substrate of this efflux transporter. P-gp can be induced by other drugs in reducing the effects if digoxin by increasing its efflux in the intestine [18].

Orange juice is taken as one of the P-gp inhibitors along with grapefruit juice which come under the 3rd generation P-gp inhibitors. The components of the orange juice are sucrose, narirutin, naringin, malic acid, hydroxycinnamic acid, glucose, fructose, ferulic acid, didymin, citric acid, ascorbic acid, Hesperidin etc. Orange juice is a long lasting and perhaps irreversible inhibitor of P-gp [19]. Another P-gp inhibitor like grapefruit juice and its components 6',7' dihydroxybergamotten (DHBG), bergamot ten (BG), other furanocoumarin derivatives potently inhibits P-gp function. Fororange juice and its components, tangeretin (TAN), 3, 3',4',5,6,7,8-heptamethoxylavone (HM) and Nobiletin (NBL) inhibit P-gp (20). Ketoconazole,

an imidazole derivative which comes under the anti-fungal classification is a strong inhibitior of P-gp [21].

Hespridin which is a component of orange juice has the highest binding affinity towards the P-gp which was done through molecular docking studies. Orange juice components inhibited the transport by P-gp however their inhibitory potencies for P-gp were substrate dependent [22]. The studies performed through the basal to apical transport and uptake of digoxin with MDR1 transfectants which showed that digoxin was transported by P-gp and by using the LLC-GA5-COL150 porcine kidney epithelial cells [23].

The steady uptake of digoxin in porcine kidney epithelial cell line transfected with human MDR1 cDNA and LLC-GA5-COL150 respectively was decreased similarly by 50% ethyl acetate extract of orange juice in MDR1 transfected cells was lower than that by 20 micrometer CysA [24].

Materials and Methods

Insilico Method:

The 3D structure of the human P-gp was predicted from the peptide by molecular threading using default settings. The Structural Analysis and Verification Server and the PDB were used to assess the stereo - chemical quality of these structures. The Molecular structure of P-gp in a transport cycle have been investigated using a variety of methods, including Antibody binding, tryptophan fluorescence, luminescence, double electron - electron resonance, electron microscopy, X- Ray Crystallography [25]. The Properties of certain components have been identified through various sources. The properties of P-gp through (http://www3.rcsb.org/ligand/PGP) [26].

Digoxin through (http://pubchem.ncbi.nlm.nih.gov/compound/Digoxin) [27]

Orange juice through (http://pubchem.ncbi.nlm.nih.gov/compound/Orange-I) [28]

Ketoconazole through (http://pubchem.ncbi.nlm.nih.gov/compound/Ketoconazole) [29]

Molecular docking has been performed to "predict the highest binding affinity to P gp with ligands of orange juice and ligands of ketoconazole" [30].

Results and Discussion

Results of molecular docking are

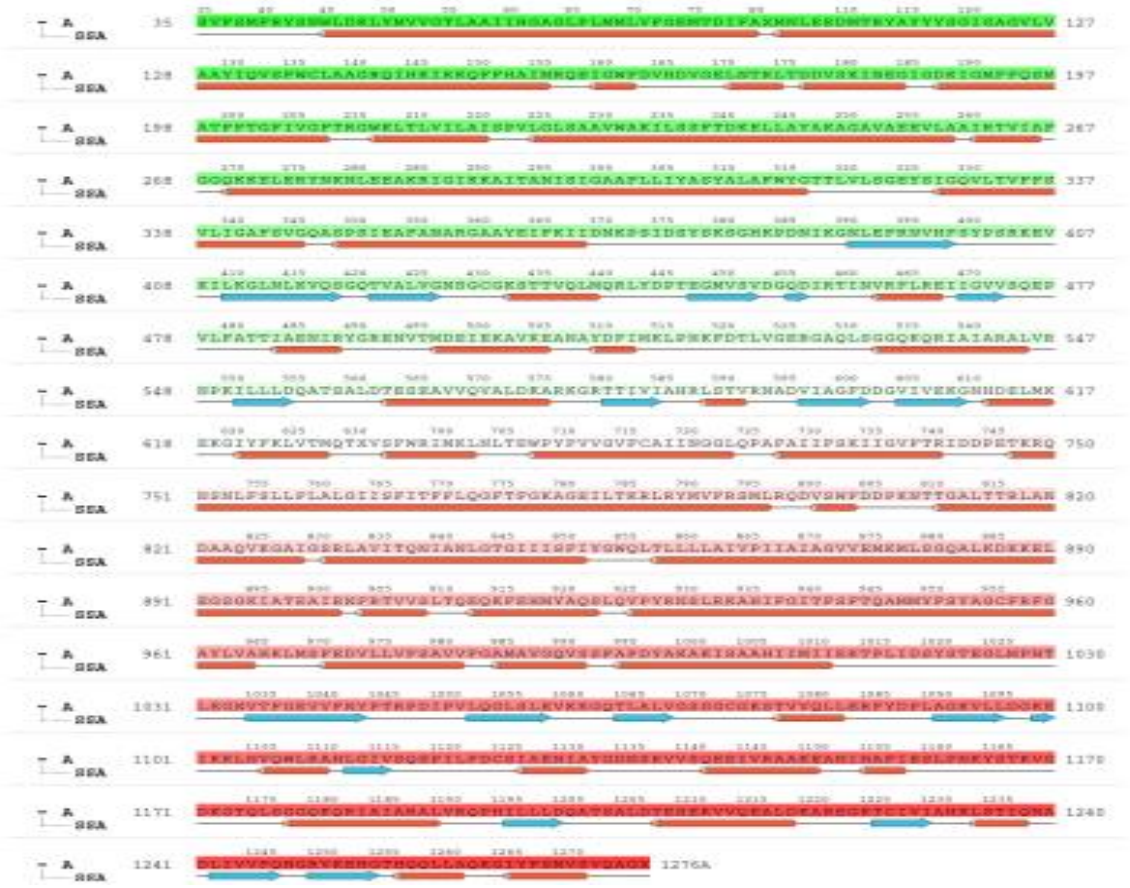

Figure 1 - Protein sequence alignment of P-glycoprotein (P-gp) showing various domains. Green regions indicate the transmembrane domains, red regions highlight the nucleotide-binding domains (NBDs), and blue segments represent specific functional motifs involved in ATP hydrolysis.

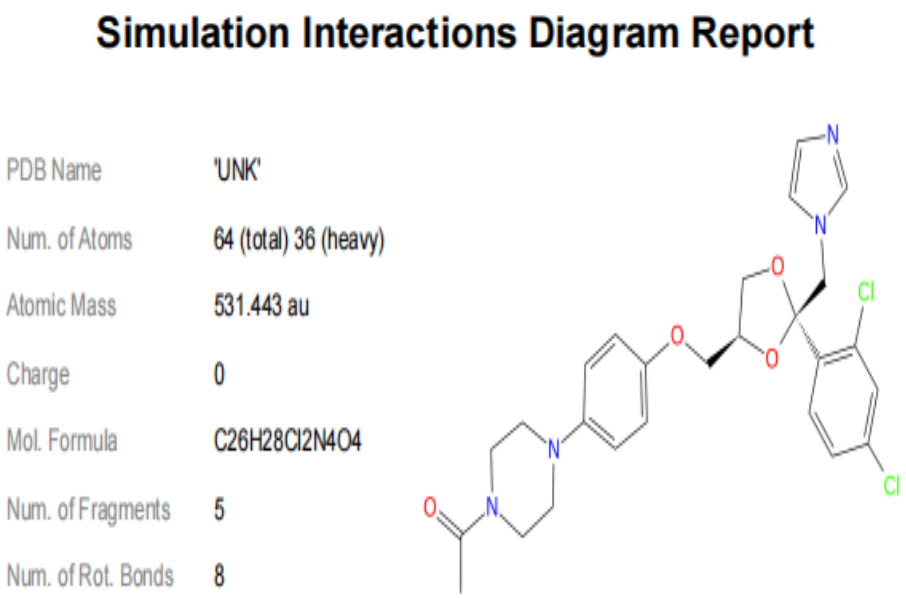

Figure 2 - Molecular structure of the compound "UNK" as identified in the PDB database.

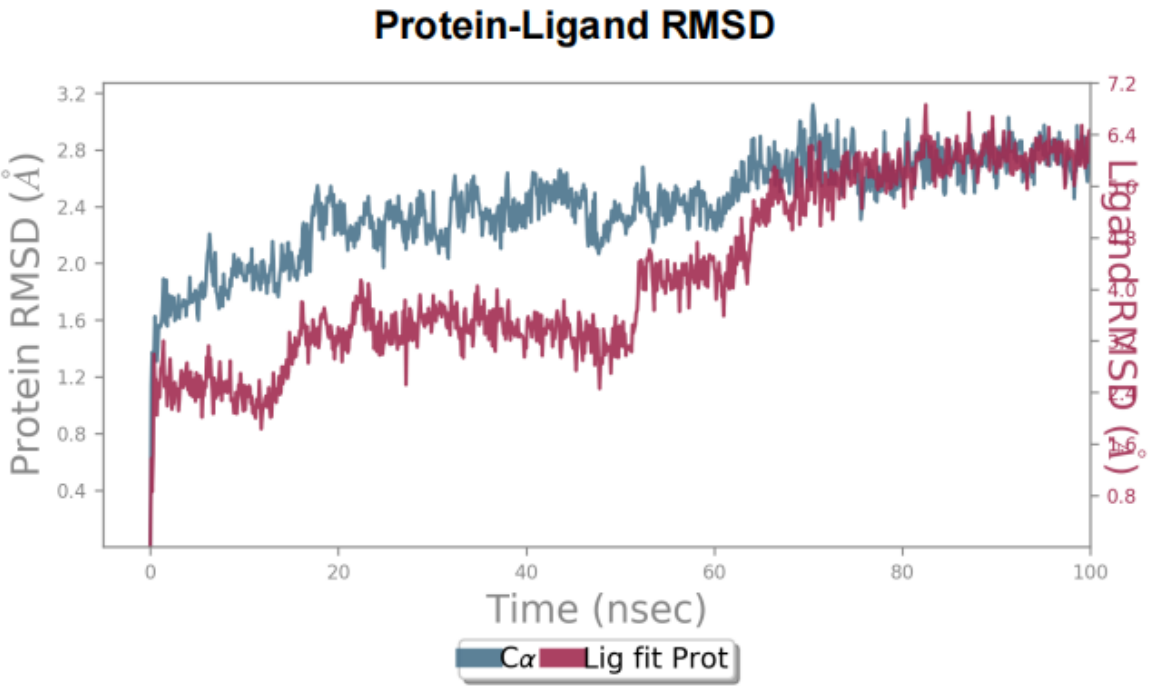

Figure 3 - Protein-Ligand Root Mean Square Deviation (RMSD) over time. The plot shows the fluctuation of Protein RMSD (blue) and Ligand RMSD (red) in Ångströms (Å) over a

simulation period of 100 nanoseconds (nsec). The protein is represented by Cα, and the ligand is fitted to the protein.

The Root Mean Square Deviation (RMSD) is used to measure the average change in displacement of a selection of atoms for a particular frame with respect to a reference frame. It is calculated for all frames in the trajectory. The RMSD for frame *x* is:

$$RMSD_x = \sqrt{\frac{1}{N}\sum_{i=1}^{N}(r_i'(t_x)) - r_i(t_{ref}))^2}$$

The Root Mean Square Fluctuation (RMSF) is useful for characterizing local changes along the protein chain. The RMSF for residue *i* is:

$$RMSF_i = \sqrt{\frac{1}{T}\sum_{t=1}^{T} < (r_i'(t)) - r_i(t_{ref}))^2 >}$$

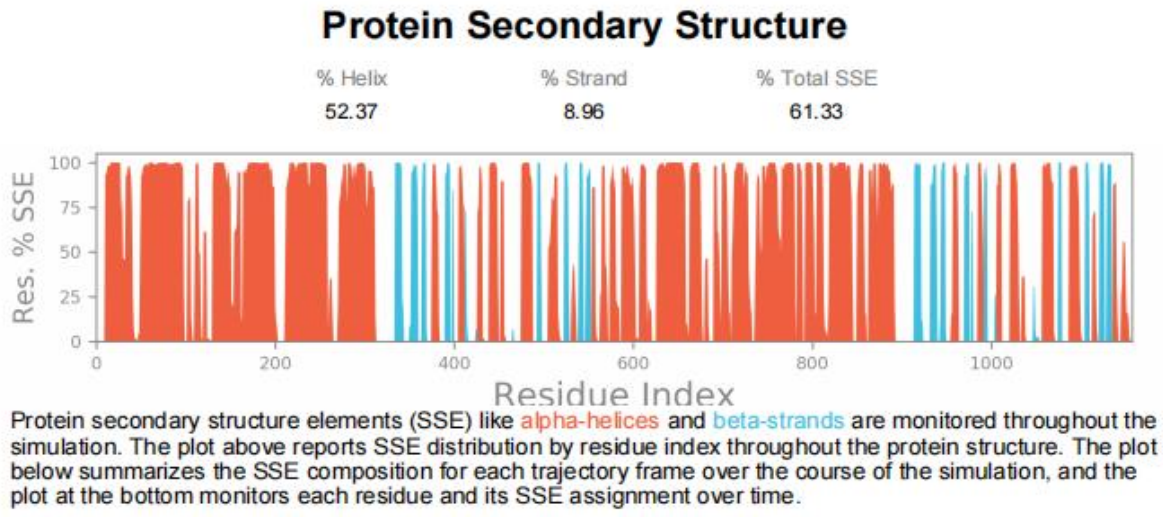

Protein secondary structure elements (SSE) like alpha-helices and beta-strands are monitored throughout the simulation. The plot above reports SSE distribution by residue index throughout the protein structure. The plot below summarizes the SSE composition for each trajectory frame over the course of the simulation, and the plot at the bottom monitors each residue and its SSE assignment over time.

Figure 4 - Protein Secondary Structure

The figure shows the distribution of secondary structure elements (SSE) like alpha-helices and beta-strands monitored throughout the simulation.

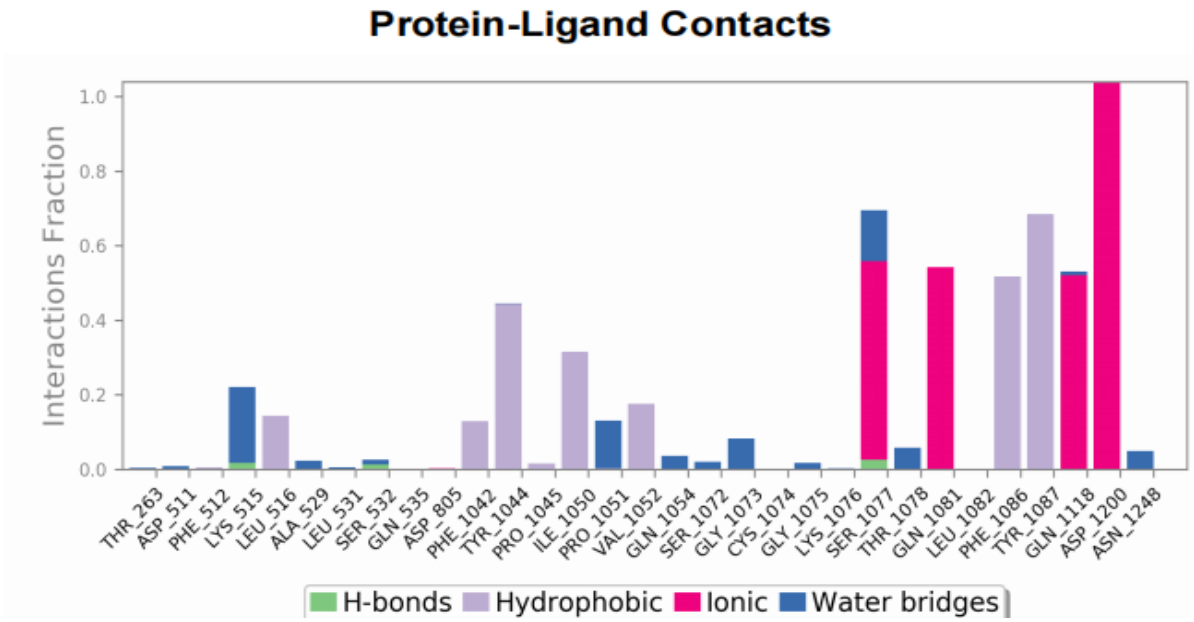

Figure 5 - Protein-Ligand Contacts

This figure illustrates the fraction of different types of interactions between specific protein residues and the ligand. The types of contacts include hydrogen bonds (H-bonds), hydrophobic interactions, ionic interactions, and water bridges, represented by green, purple, pink, and blue bars, respectively. Residues involved in these interactions are labeled along the x-axis, with the interaction fractions shown on the y-axis.

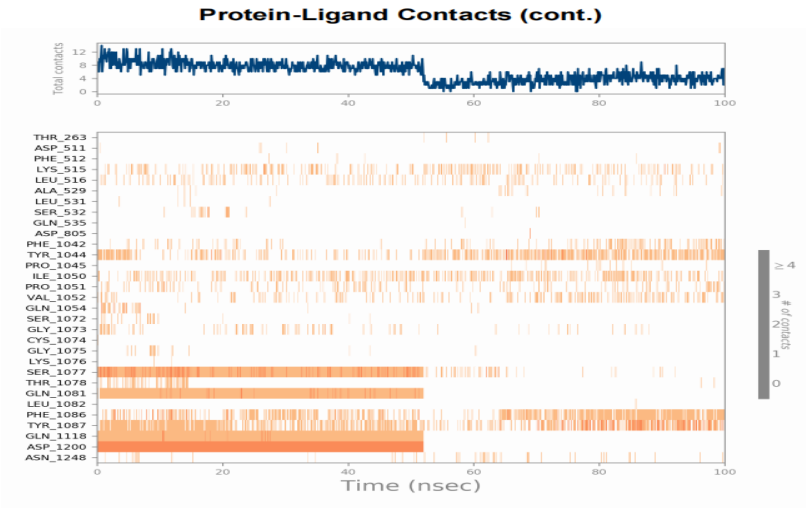

Figure 6 - Protein-Ligand Contacts over Time. The top panel shows the total number of contacts between the protein and ligand throughout a 100-nanosecond simulation.

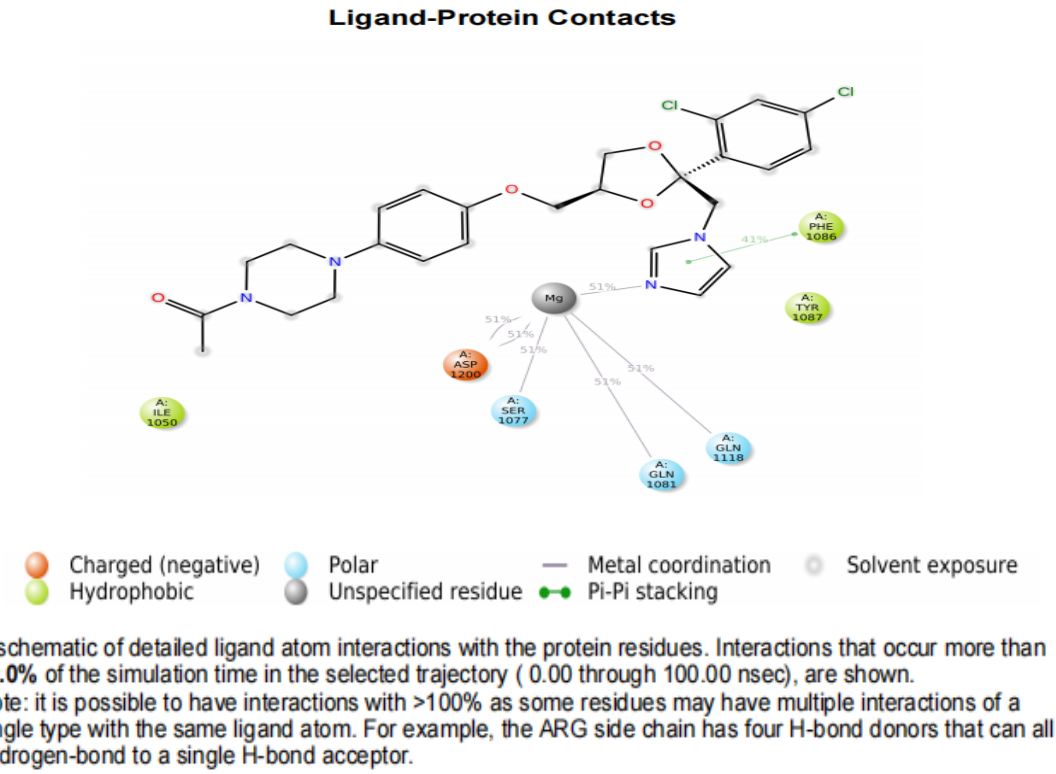

Figure 7 - Ligand-Protein Interaction Map. This diagram shows the key residues involved in interactions between the ligand and the protein. Residue contacts are color-coded, with their respective frequencies of interaction labeled in percentages. The magnesium ion (Mg) plays a central role, forming multiple contacts with residues such as ASP1200, SER1077, GLN1081, and GLN1118, all with 51% contact frequency. Other significant contacts include PHE1086 (41%) and TYR1087.

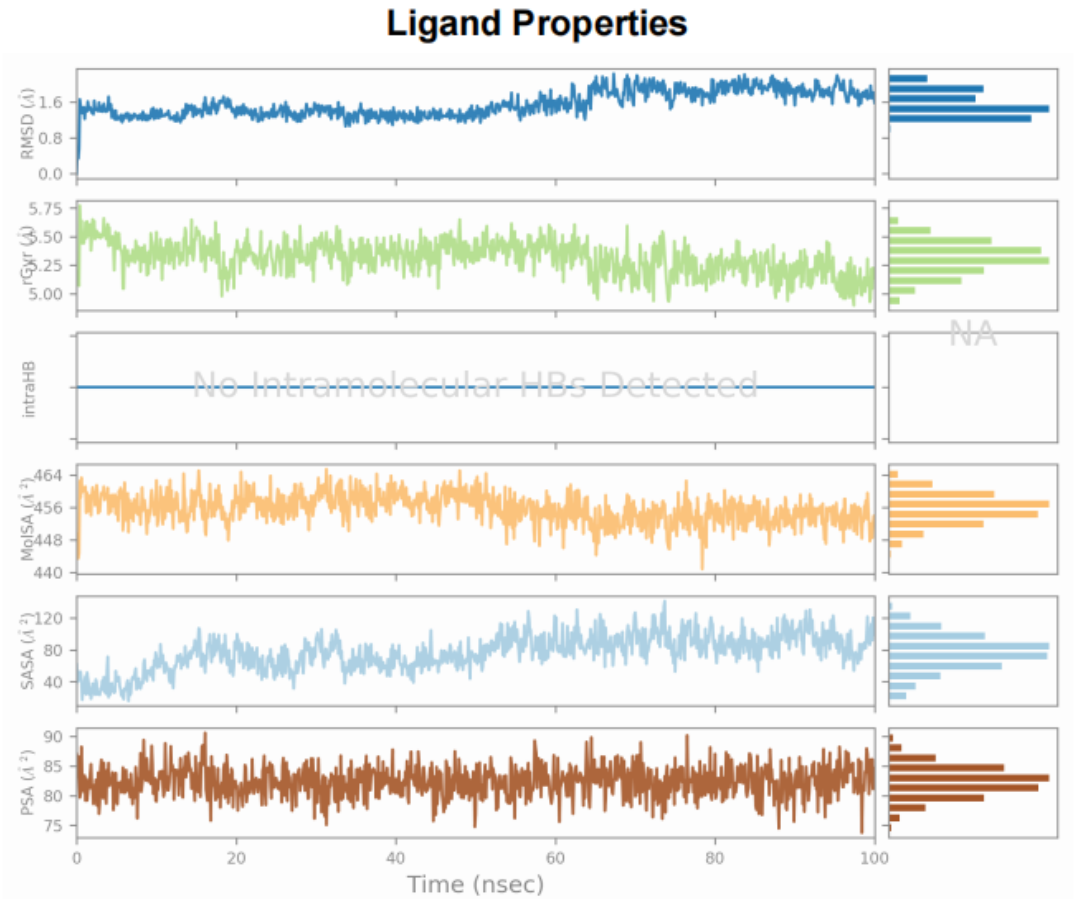

Figure 8 - Ligand Properties Over a 100-Nanosecond Simulation. The plots represent various ligand properties monitored during the simulation. From top to bottom: Root Mean Square Deviation (RMSD), Radius of Gyration (rGY), Intra-ligand Hydrogen Bonds (IntraHB), Molecular Surface Area (MoSA), Solvent Accessible Surface Area (SASA), and Polar Surface Area (PSA). Each plot tracks changes over time (in nanoseconds), with histograms on the right showing the distribution of values across the simulation.

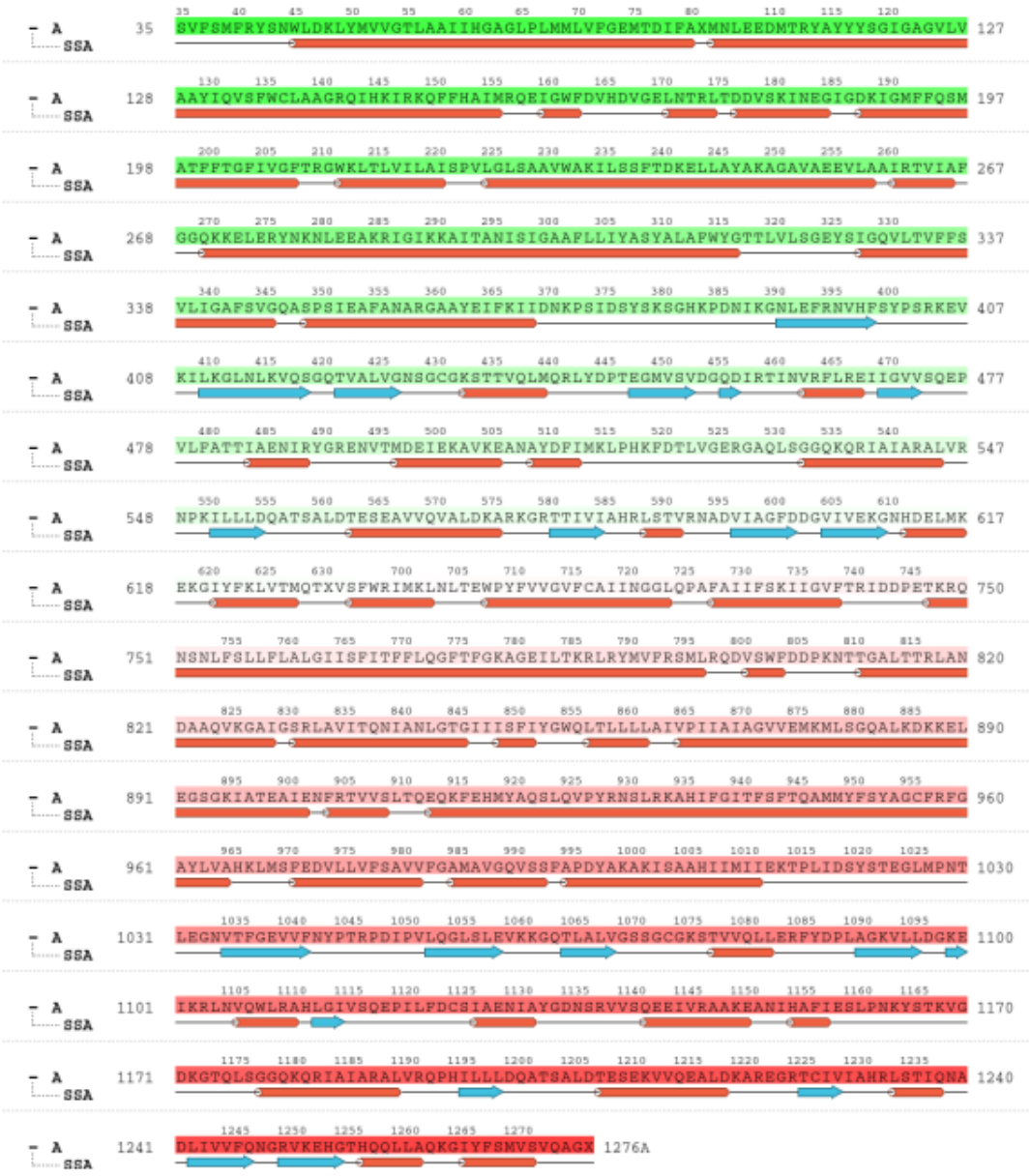

Figure 9 - Sequence alignment of two protein sequences labeled as "A" and "88A."

PDB Name	'UNK'
Num. of Atoms	93 (total) 53 (heavy)
Atomic Mass	756.675 au
Charge	0
Mol. Formula	C33H40O20
Num. of Fragments	4
Num. of Rot. Bonds	22

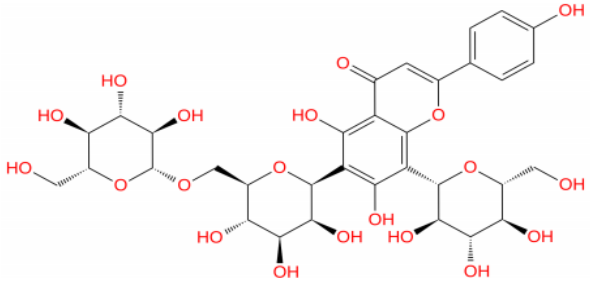

Counter Ion/Salt Information

Type	Num.	Concentration [mM]	Total Charge
Cl	80	66.570	-80
Na	61	50.759	+61

Figure 10 - Molecular structure and details of the unknown ligand 'UNK'. The figure shows the molecular formula C33H40O20 with an atomic mass of 756.675 atomic units (au). The total number of atoms is 93, with 53 heavy atoms.

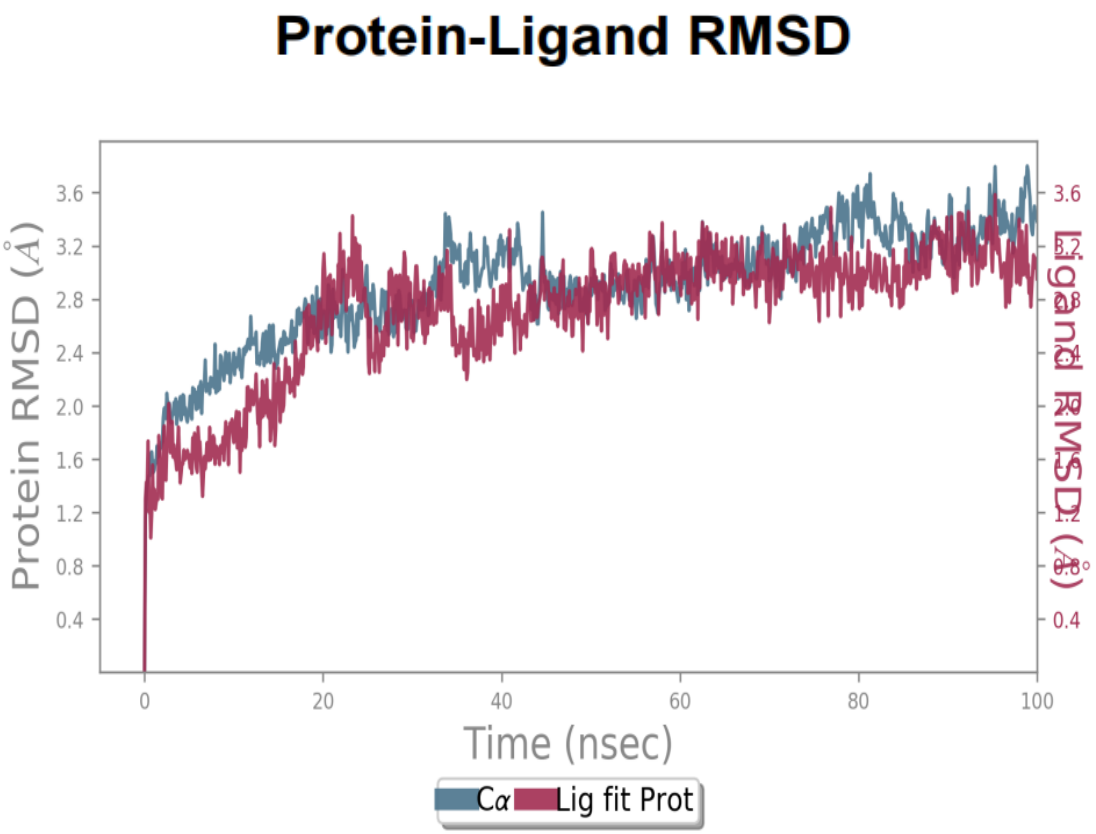

Figure 11 - Time-dependent RMSD analysis of Protein-Ligand complex. The plot shows the Root Mean Square Deviation (RMSD) of the protein's Cα atoms (blue line) and the

ligand's fit on the protein (red line) over the course of a 100-nanosecond molecular dynamics simulation. The RMSD values are measured in Ångströms (Å) as a function of time in nanoseconds (nsec)

The Root Mean Square Deviation (RMSD) is used to measure the average change in displacement of a selection of atoms for a particular frame with respect to a reference frame. It is calculated for all frames in the trajectory. The RMSD for frame *x* is:

$$RMSD_x = \sqrt{\frac{1}{N}\sum_{i=1}^{N}(r_i'(t_x)) - r_i(t_{ref}))^2}$$

Protein secondary structure elements (SSE) like alpha-helices and beta-strands are monitored throughout the simulation. The plot above reports SSE distribution by residue index throughout the protein structure. The plot below summarizes the SSE composition for each trajectory frame over the course of the simulation, and the plot at the bottom monitors each residue and its SSE assignment over time.

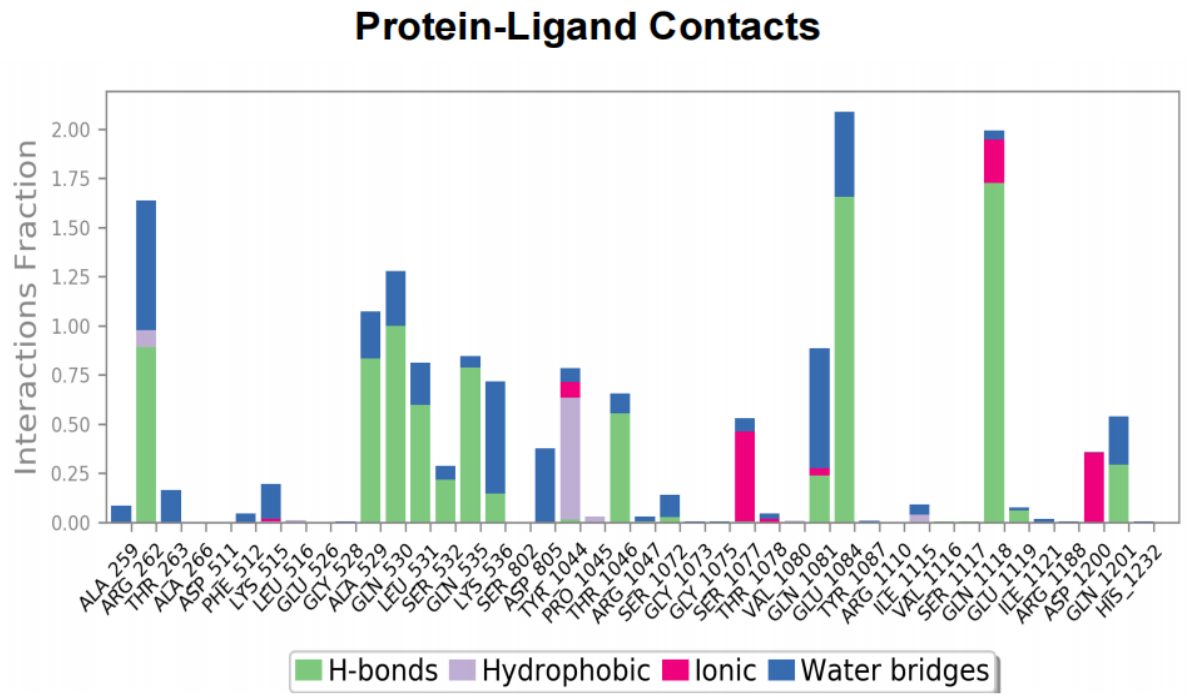

Figure 12 - Protein-ligand contacts observed during the simulation. The bar graph displays the fraction of various types of interactions (H-bonds, hydrophobic interactions, ionic bonds, and water bridges) between the ligand and specific protein residues. The residues are listed along the x-axis, while the interaction fraction is shown on the y-axis.

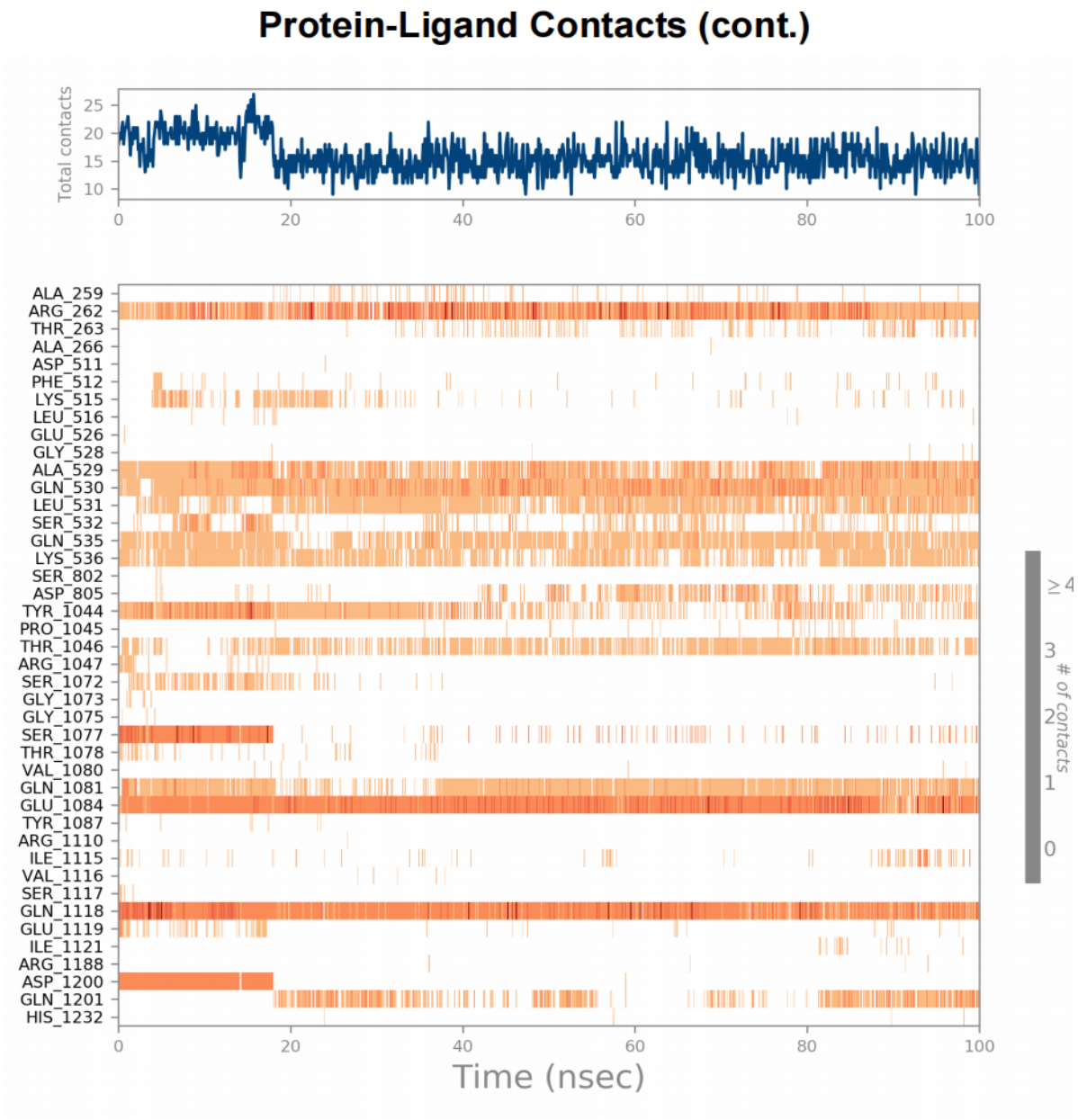

Figure 13. Time evolution of protein-ligand contacts. The top panel shows the total number of contacts between the protein and the ligand over the course of the 100-nanosecond simulation. The bottom panel is a heatmap displaying the number of contacts between the ligand and individual residues of the protein, as a function of time. The intensity of the color corresponds to the number of contacts, with darker shades representing more contacts.

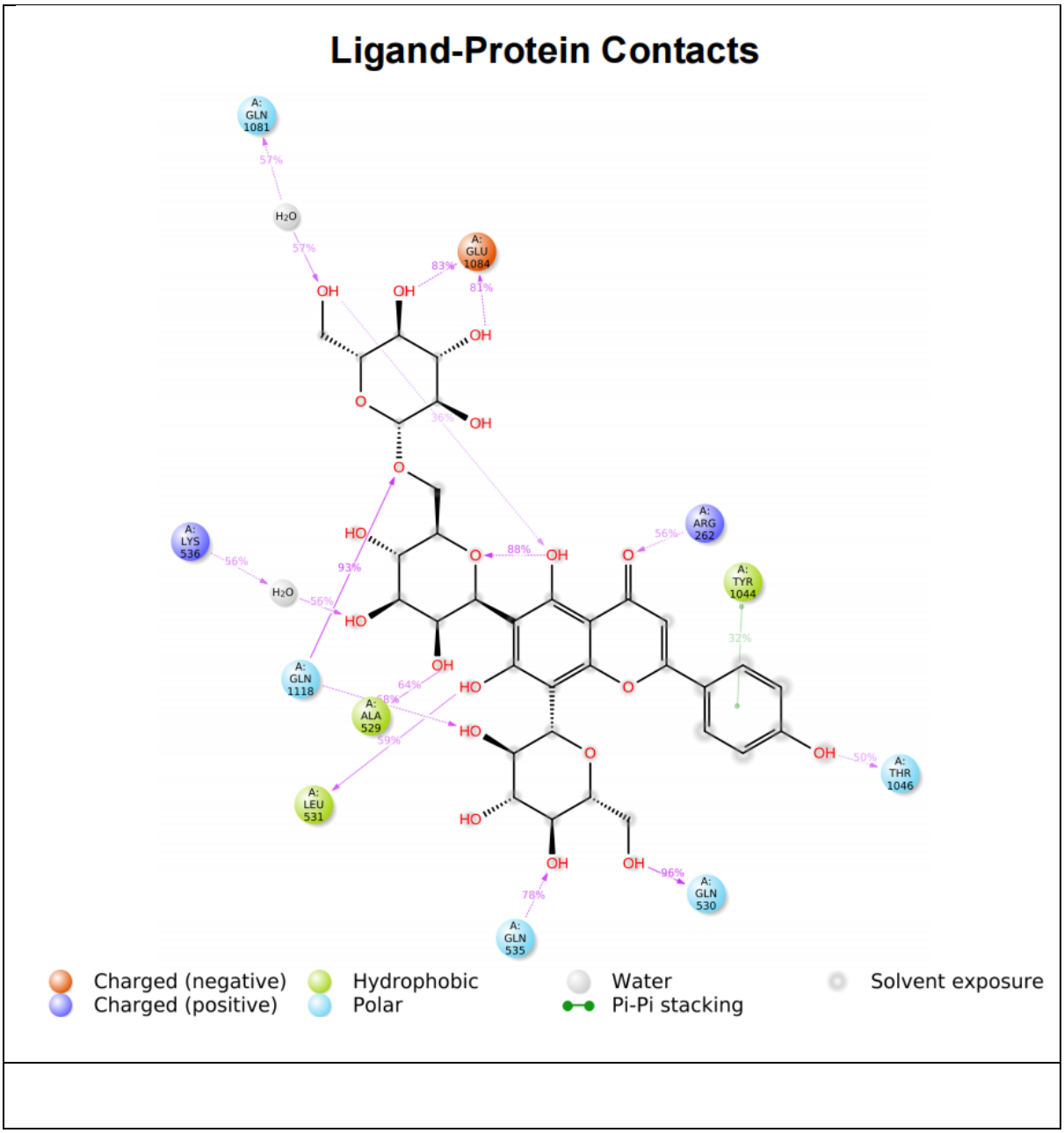
Ligand-Protein Contacts
A: GLN 1081
57%
H2O
57%
A: GLU 1084
83%
81%
OH
OH
OH
O
OH
36%
O
A: LYS 536
56%
H2O
56%
93%
HO
HO
O
88%
OH
O
56%
A: ARG 262
A: TYR 1044
32%
A: GLN 1118
64%
58%
A: ALA 529
59%
OH
HO
HO
O
O
OH
50%
A: THR 1046
A: LEU 531
HO
OH
OH
96%
A: GLN 530
78%
A: GLN 535
Charged (negative)
Charged (positive)
Hydrophobic
Polar
Water
Pi-Pi stacking
Solvent exposure

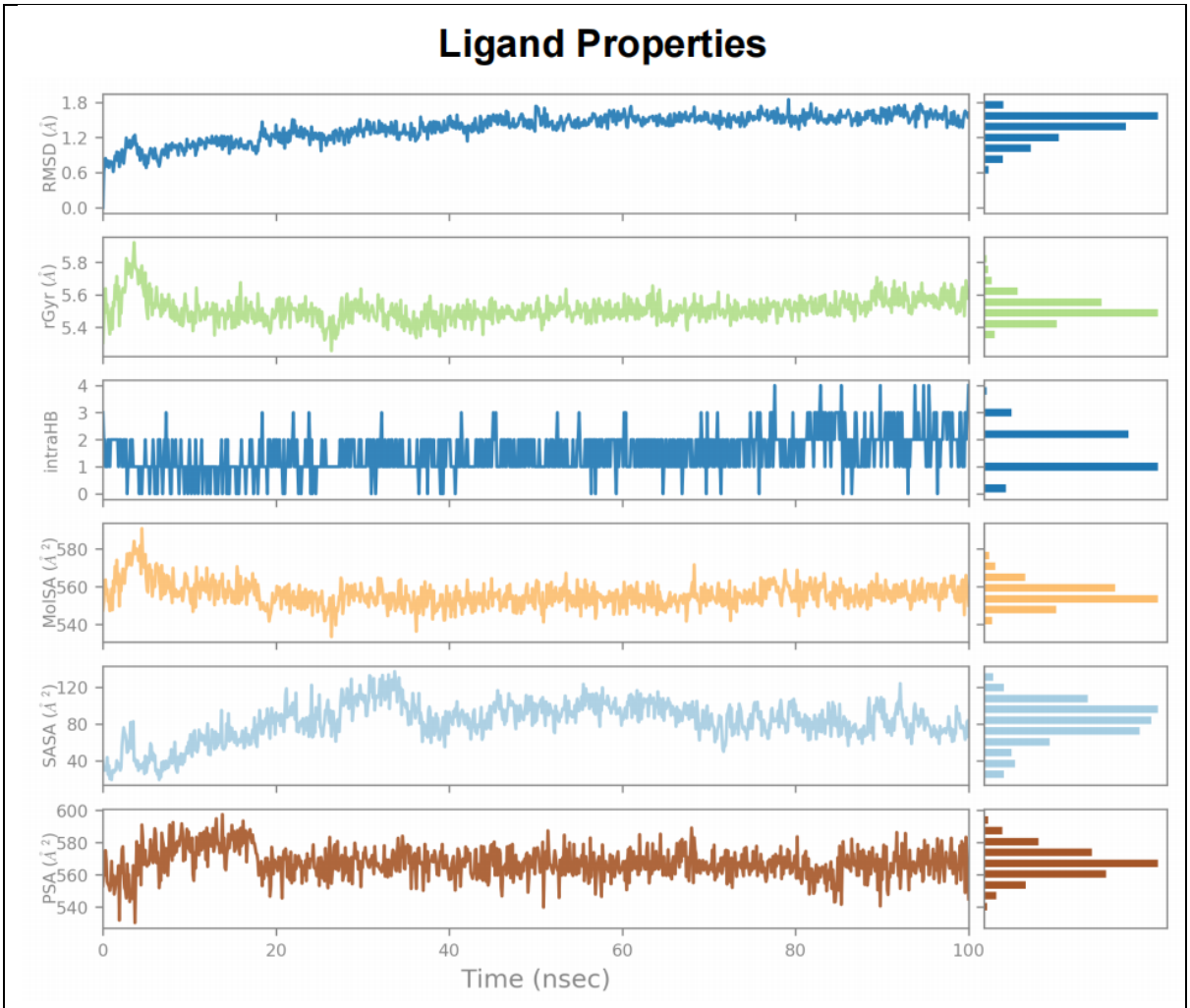
Ligand Properties
RMSD (Å)
rGyr (Å)
intraHB
MolSA (Å²)
SASA (Å²)
PSA (Å²)
Time (nsec)

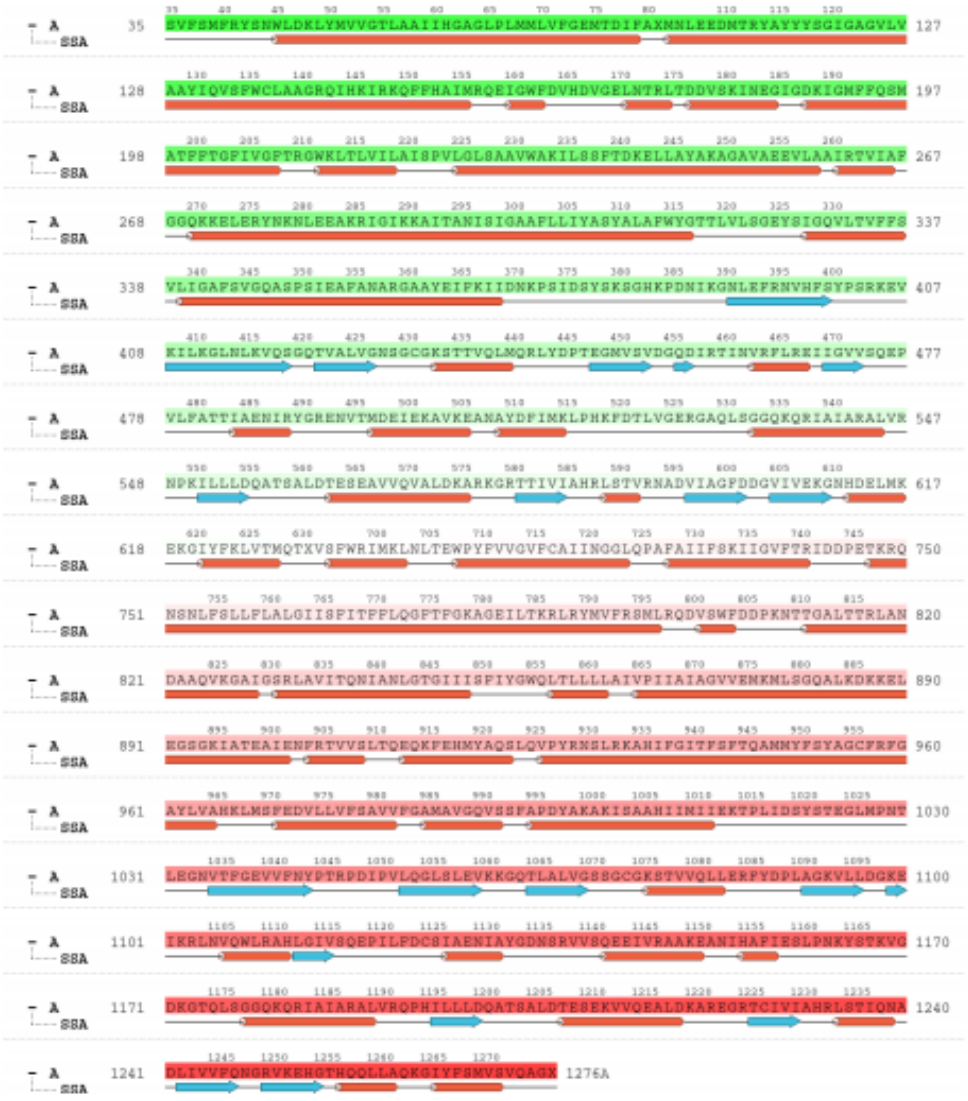

PDB Name	'ATP'
Num. of Atoms	43 (total) 31 (heavy)
Atomic Mass	503.154 au
Charge	-4
Mol. Formula	C10H12N5O13P3
Num. of Fragments	2
Num. of Rot. Bonds	11

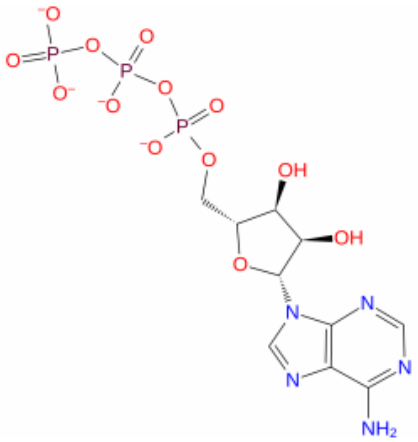

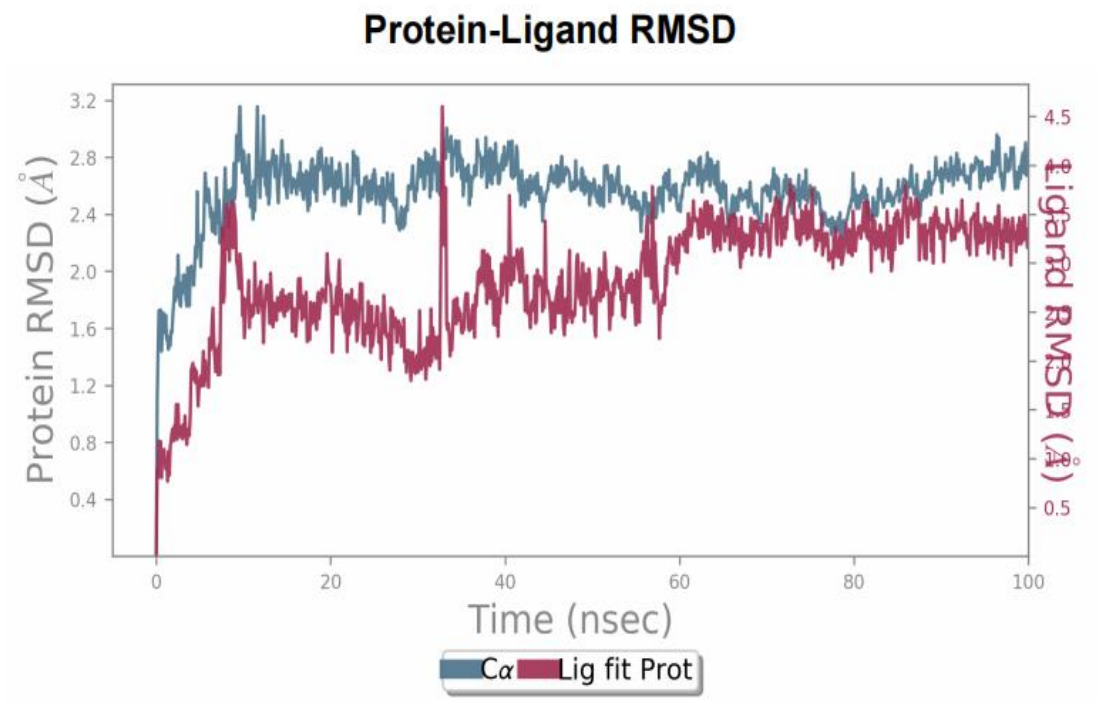

The Root Mean Square Deviation (RMSD) is used to measure the average change in displacement of a selection of atoms for a particular frame with respect to a reference frame. It is calculated for all frames in the trajectory. The RMSD for frame *x* is:

$$RMSD_x = \sqrt{\frac{1}{N}\sum_{i=1}^{N}(r_i'(t_x)) - r_i(t_{ref}))^2}$$

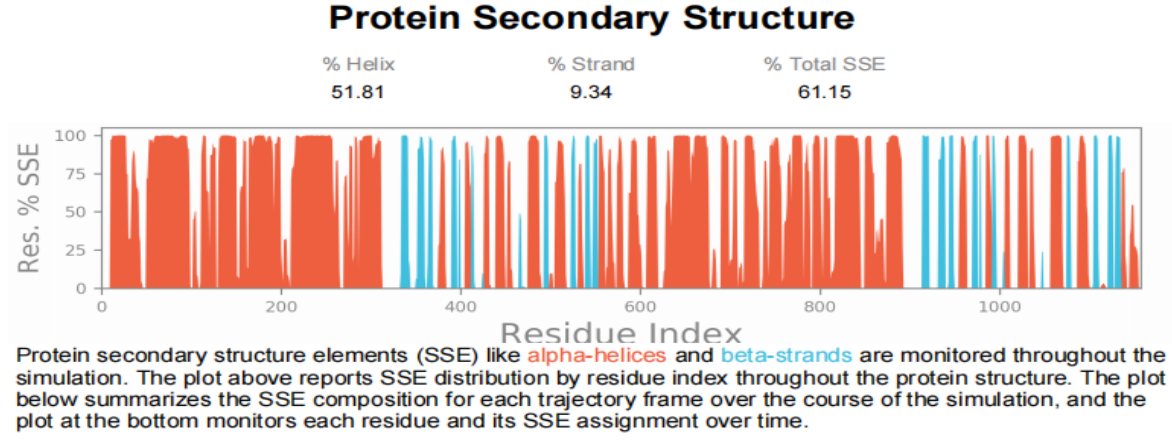

Protein secondary structure elements (SSE) like alpha-helices and beta-strands are monitored throughout the simulation. The plot above reports SSE distribution by residue index throughout the protein structure. The plot below summarizes the SSE composition for each trajectory frame over the course of the simulation, and the plot at the bottom monitors each residue and its SSE assignment over time.

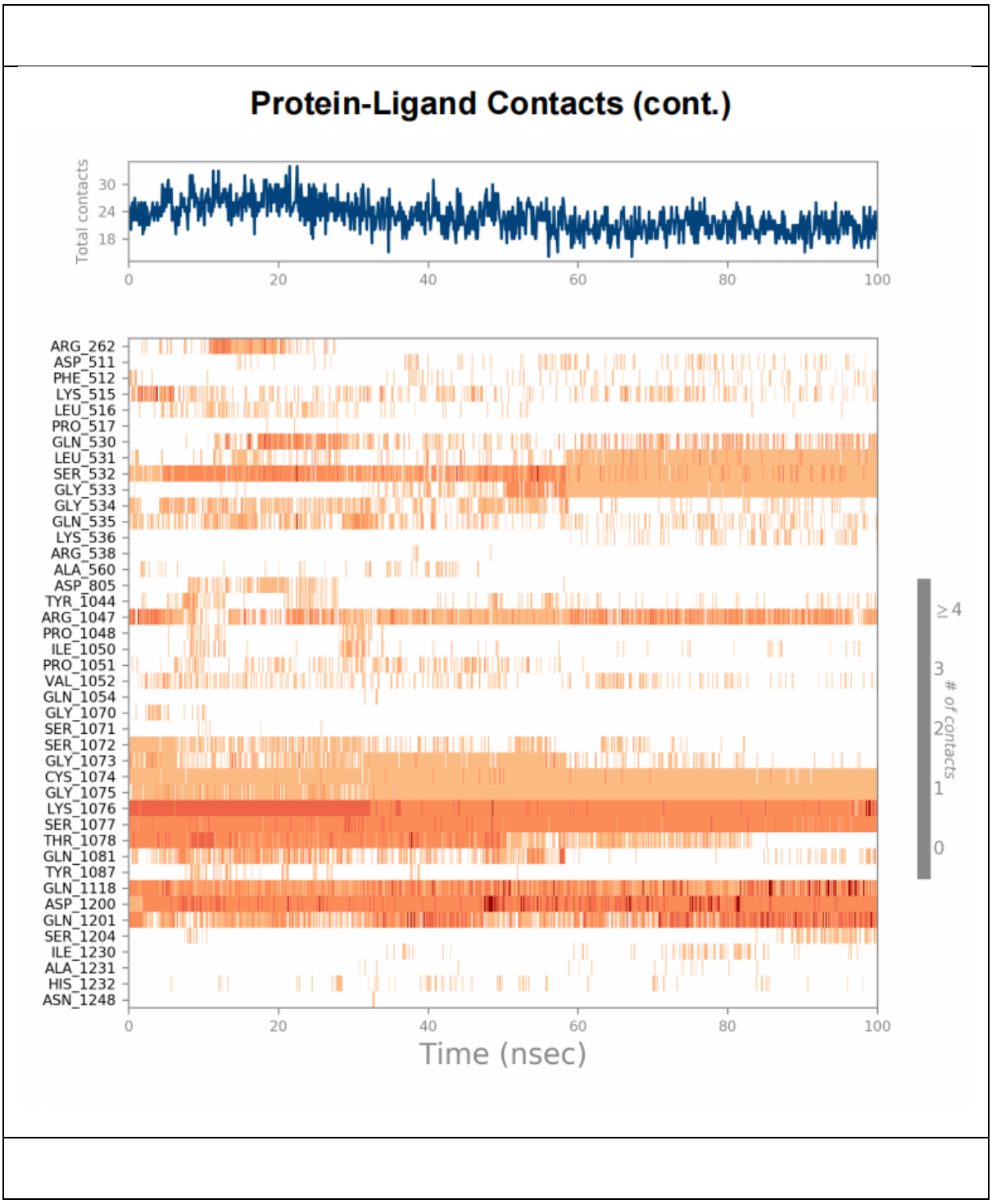
Protein-Ligand Contacts (cont.)
Total contacts
30
24
18
0
20
40
60
80
100
ARG_262
ASP_511
PHE_512
LYS_515
LEU_516
PRO_517
GLN_530
LEU_531
SER_532
GLY_533
GLY_534
GLN_535
LYS_536
ARG_538
ALA_560
ASP_805
TYR_1044
ARG_1047
PRO_1048
ILE_1050
PRO_1051
VAL_1052
GLN_1054
GLY_1070
SER_1071
SER_1072
GLY_1073
CYS_1074
GLY_1075
LYS_1076
SER_1077
THR_1078
GLN_1081
TYR_1087
GLN_1118
ASP_1200
GLN_1201
SER_1204
ILE_1230
ALA_1231
HIS_1232
ASN_1248
Time (nsec)
≥ 4
3
2
1
0
# of contacts

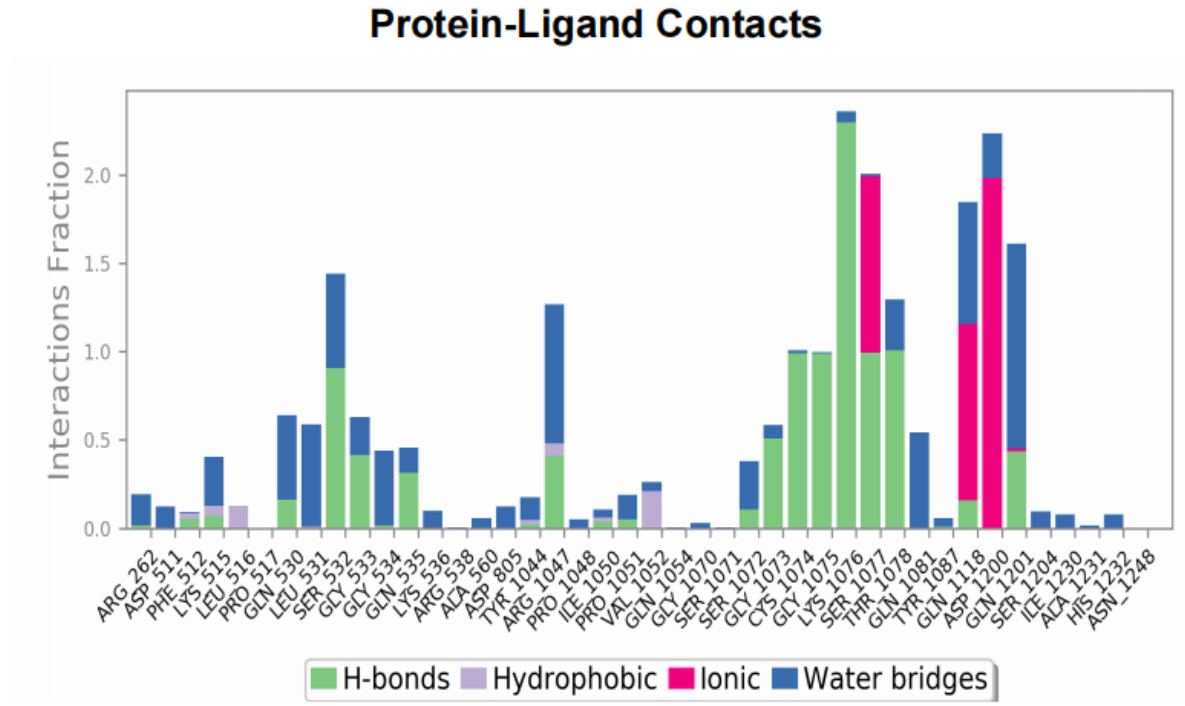
Protein-Ligand Contacts
Interactions Fraction
0.0
0.5
1.0
1.5
2.0
ARG 262
ASP 511
PHE 512
LYS 515
LEU 516
PRO 517
GLN 530
LEU 531
SER 532
GLY 533
GLY 534
GLN 535
LYS 536
ARG 538
ALA 560
ASP 805
TYR 1044
ARG 1047
PRO 1048
ILE 1050
PRO 1051
VAL 1052
GLN 1054
GLY 1070
SER 1071
SER 1072
GLY 1073
CYS 1074
GLY 1075
LYS 1076
SER 1077
THR 1078
GLN 1081
TYR 1087
GLN 1118
ASP 1200
GLN 1201
SER 1204
ILE 1230
ALA 1231
HIS 1232
ASN 1248
H-bonds
Hydrophobic
Ionic
Water bridges

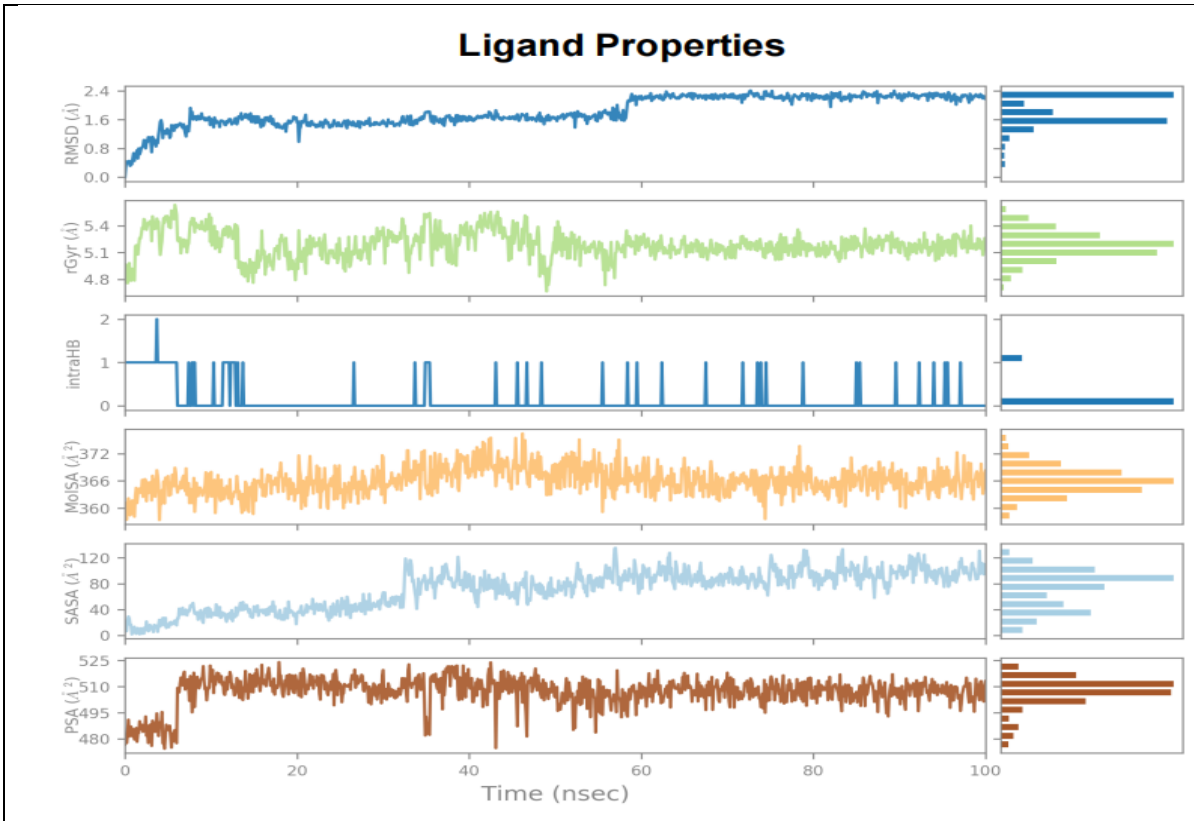
Ligand Properties
RMSD (Å)
rGyr (Å)
intraHB
MolSA (Å²)
SASA (Å²)
PSA (Å²)
Time (nsec)
0
20
40
60
80
100

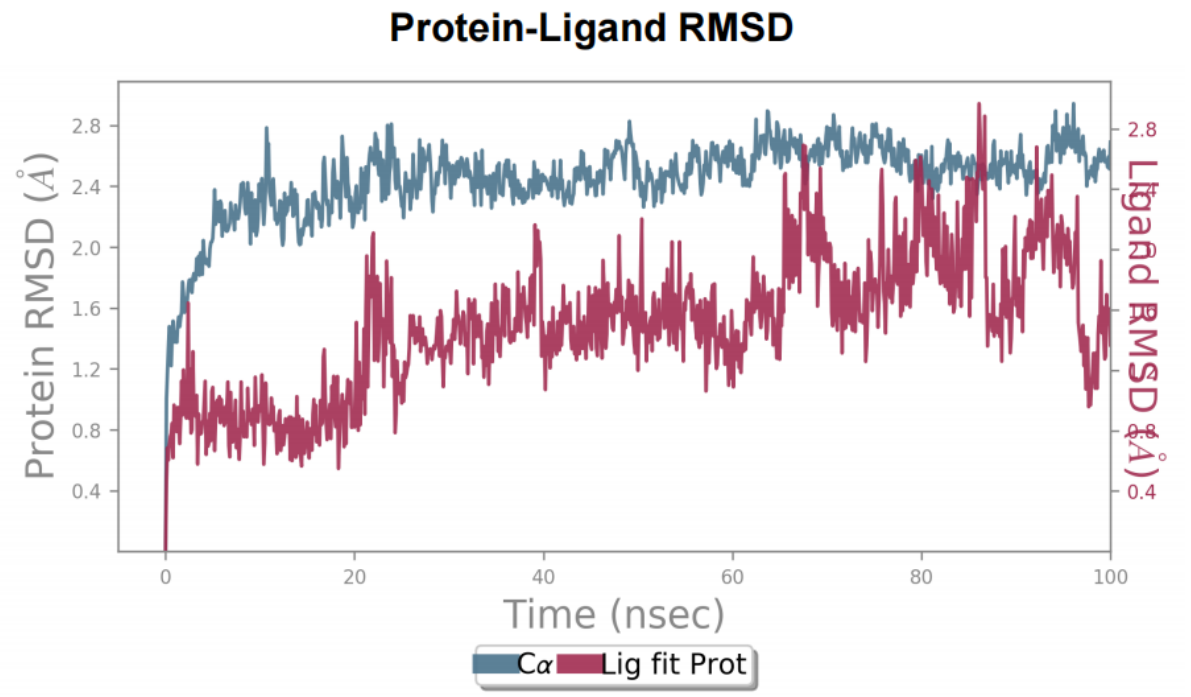

The Root Mean Square Deviation (RMSD) is used to measure the average change in displacement of a selection of atoms for a particular frame with respect to a reference frame. It is calculated for all frames in the trajectory. The RMSD for frame *x* is:

$$RMSD_x = \sqrt{\frac{1}{N}\sum_{i=1}^{N}(r_i'(t_x)) - r_i(t_{ref}))^2}$$

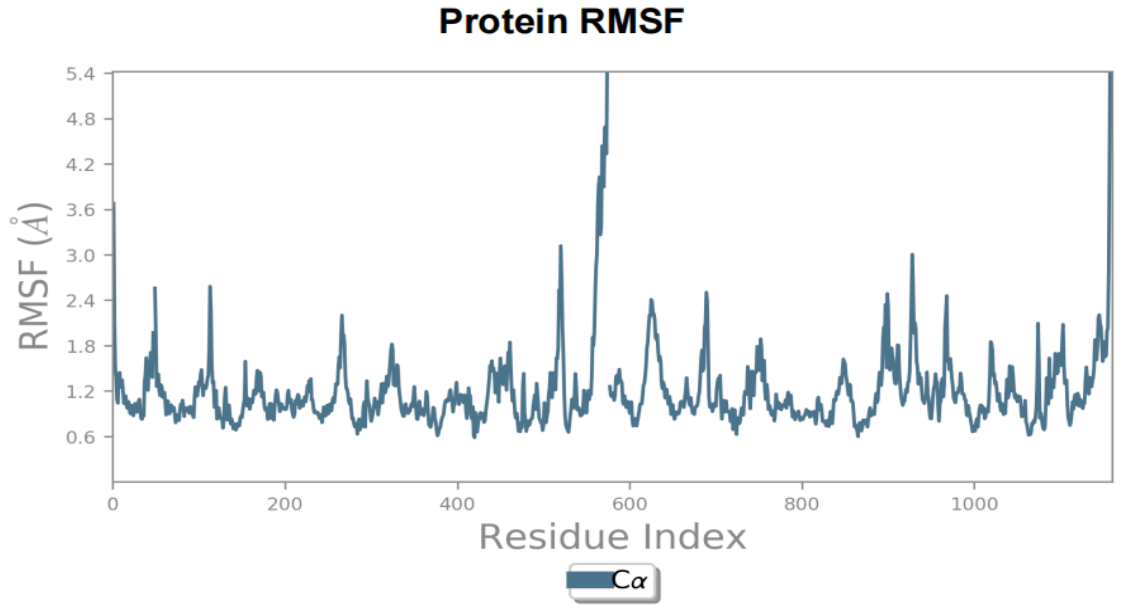

The Root Mean Square Fluctuation (RMSF) is useful for characterizing local changes along the protein chain. The RMSF for residue *i* is:

$$RMSF_i = \sqrt{\frac{1}{T}\sum_{t=1}^{T} < (r_i'(t)) - r_i(t_{ref}))^2 >}$$

TITLE	ENTRY ID	GLIDE GSCORE	MMGBSA Dg BIND	MMGBSA dG BIND COULOMB	MMGBSA dG BIND HBOND	MMGBSA dG BIND LIPO	MMGBSA dG BIND vDW
44257711 =Vicenin-2,6”-O-Glucoside	49	-13.803	-174.43	-182.30	-12.97	-42.48	-98.02
44257711 =Vicenin -2,6”-O-Glycoside	50	-13.754	--102.44	-45.37	-10.07	-9.73	14.91
442431 =Narirutin	51	-11.675	-82.26	-153.69	-14.74	-27.14	-48.22
42428 =Naringen	52	-11.652	-90.16	-130.91	-13.82	-29.47	-41.94
16760075 =Diclymin	53	-10.237	-90.51	-238.30	-13.89	-29.27	-47.85
54670067 =L-Ascorbic acid	54	-10.112	-103.54	-115.73	-8.42	-23.23	-30.55
5988 =Sucrose	55	-8.667	-26.36	-32.05	-11.82	-31.44	-27.49
525 =Malic Acid	56	-7.146	-76.57	-146.99	-9.92	-19.29	-54.96

5793 =D-Glyco pyranose	57	-7.059	-107.14	-188.76	-15.20	-38.42	-57.85
2724385 =Digoxin	58	-6.803	-113.23	-171.62	-10.02	-48.25	-84.89
135398658 =Folic Acid	59	-5.935	-26.99	-23.18	-15.10	-30.26	-43.73
311 =Citric acid	60	-5.897	-57.66	-169.73	-14.39	-20.37	-33.01
2723872	61	-5.389	-77.05	-126.32	-8.92	-24.79	-48.90
445858 =Ferulic Acid (trans)	62	-4.946	-103.23	-115.97	-12.78	-29.75	-22.42
17100 =Alpha-Terpineol	63	-4.850	-86.58	-141.24	-11.58	-36.08	-48.40
637542 =4-Hydroxy Cinnamic acid	64	-4.736	-50.85	-97.77	-14.13	-26.61	-68.34
5291 =Imatinib	65	-4.582	-26.83	-55.45	-0.10	-25.98	-37.72
3823 =Ketoconazole	66	-4.528	-114.36	-160.64	-8.06	-48.88	-88.85

22311 =Limonene	67	-2.622	-51.89	-49.34	-4.11	-15.82	23.39
6COV-4-hbond-opt_molecule3 =ATP	68	-20.389	-61.53	-239.41	-15.10	-17.30	-78.40

Since MMGBSA dG Bind of Vicenin -2,6”-O-Glucoside is having the highest binding energy (-174.43) it is used as a potent inhibitor of the P-gp protein.

Conclusion

The p-gp protein properties were read in the PDB and was found to have the expression system in homosapiens. The molecular docking method was used to find the binding energy of the orange juice components with the p-gp protein. The results showed that Vicenin-2,6”-O-Glucoside has the highest binding energy towards the P-gp protein. Hence Vicenin-2,6”-O-Glucoside was found to be a good P-gp inhibitor.

Acknowledgements

We would like to express our gratitude to Ms. J Rebekal, Ms. Racheal Swetha R, Ms. Raghava Bhavana Shreya, Ms. Priyadharseni M S & Ms. Kelsang Dolma for invaluable support and assistance during the study.

References

1. Dano, K. (1973). Energy-dependent drug accumulation in tumor cells. Journal of Cellular Physiology, 82(2), 199–204.
2. Juliano, R., and Ling, V. (1976). The permeability glycoprotein: A new perspective on drug resistance. Molecular Pharmacology, 12(4), 599–608.
3. Kim, Y., and Chen, J. (2018). Molecular structure of human P-glycoprotein in the ATP-bound outward-facing conformation. Science, 359, 915–919.

4. Germann, D., Shah, P., and Ludwig, R. (2015). Evaluation of natural inhibitors of P-glycoprotein using in-silico and in-vitro methods. Biochemical Pharmacology, 89(2), 349–356.
5. Fischer, H., and Müller, D. (2005). Pharmacogenetics of P-glycoprotein: Implications for drug therapy. Pharmacogenomics Journal, 5(4), 236–243.
6. Meyer, J. S., and Jansen, S. (2014). Molecular mechanisms of P-glycoprotein-mediated drug transport. Drug Metabolism Reviews, 46(1), 105–134.
7. Benet, L. Z., and P-glycoprotein. (2002). The influence of P-glycoprotein on drug transport. Drug Metabolism and Disposition, 30(2), 130–132.
8. Thiebaut, F., and Deeley, R. G. (2000). Multidrug resistance and P-glycoprotein: A review. Cancer Biology & Therapy, 1(4), 299–305.
9. Gottfried, J. R., and Wilson, R. J. (2011). P-glycoprotein: Mechanisms and implications in drug development. Journal of Pharmaceutical Sciences, 100(4), 1020–1033.
10. Ushigome, F., Honda, Y., and Koyabu, N. (2004). Effects of grapefruit juice and orange juice on P-glycoprotein-mediated drug transport. British Journal of Pharmacology, 143(7), 856–864.
11. Ambudkar, S. V., and Dey, S. (2009). P-glycoprotein: A complex transporter with diverse substrates. Journal of Pharmaceutical Sciences, 98(10), 3485–3500.
12. Zhou, S. F., and Wang, C. Y. (2010). Drug-drug interactions of P-glycoprotein substrates. Chinese Journal of Pharmacology and Toxicology, 24(4), 408–415.
13. Rush, C. (2015). Drug interactions involving P-glycoprotein: Implications for therapy. Clinical Pharmacology & Therapeutics, 97(2), 127–135.
14. Santos, S., and Landau, M. (2010). Mechanisms of drug resistance: P-glycoprotein and its inhibitors. Journal of Pharmaceutical Sciences, 99(4), 1675–1687.

15. Sharma, R., and Sharma, A. (2013). P-glycoprotein as a target for drug delivery. Expert Opinion on Drug Delivery, 10(3), 407–423.
16. Rocchi, P., and Polilli, E. (2009). P-glycoprotein: A key player in drug transport and resistance. Current Medicinal Chemistry, 15(3), 282–289.
17. Kannan, P., and Trivedi, P. (2014). P-glycoprotein: Current understanding and future perspectives. Clinical Pharmacokinetics, 53(8), 673–684.
18. Bunone, I., and Valli, M. (2008). P-glycoprotein: Current understanding and future directions. Current Medicinal Chemistry, 15(3), 282–289.
19. Tsvetkova, T., and Petrov, A. (2018). The impact of dietary flavonoids on P-glycoprotein transport activity. Molecules, 23(1), 220.
20. Frost, C. E., Byon, W., and Song, Y. (2015). Effect of ketoconazole on the pharmacokinetics of apixaban, an oral direct Factor Xa inhibitor. British Journal of Clinical Pharmacology, 79(5), 838–846.
21. Dano, K. (1973). Energy-dependent drug accumulation in tumor cells. Journal of Cellular Physiology, 82(2), 199–204.
22. Ambudkar, S. V., and Dey, S. (2009). P-glycoprotein: A complex transporter with diverse substrates. Journal of Pharmaceutical Sciences, 98(10), 3485–3500.
23. Germann, D., Shah, P., and Ludwig, R. (2015). Evaluation of natural inhibitors of P-glycoprotein using in-silico and in-vitro methods. Biochemical Pharmacology, 89(2), 349–356.
24. Ushigome, F., Honda, Y., and Koyabu, N. (2004). Effects of grapefruit juice and orange juice on P-glycoprotein-mediated drug transport. British Journal of Pharmacology, 143(7), 856–864.

25. Trott, O., and Olson, A. J. (2010). AutoDock Vina: Improving the speed and accuracy of docking with a new scoring function, efficient optimization, and multithreading. Journal of Computational Chemistry, 31(2), 455-461.
26. RCSB Protein Data Bank. (n.d.). Ligand: PGP. Retrieved from http://www3.rcsb.org/ligand/PGP
27. PubChem. (n.d.). Digoxin. Retrieved from http://pubchem.ncbi.nlm.nih.gov/compound/Digoxin
28. PubChem. (n.d.). Orange Juice. Retrieved from http://pubchem.ncbi.nlm.nih.gov/compound/Orange-I
29. PubChem. (n.d.). Ketoconazole. Retrieved from http://pubchem.ncbi.nlm.nih.gov/compound/Ketoconazole
30. Frisch, M. J., et al. (2016). Gaussian 16, Revision A.03. Gaussian, Inc., Wallingford, CT.